INTEGRATION OF THE PRIMITIVE BAROTROPIC MODEL OVER A SPHERICAL GEODESIC GRID

DAVID L. WILLIAMSON[1]

National Center for Atmospheric Research,[2] Boulder, Colo.

ABSTRACT

Conservative finite-difference approximations are developed for the primitive barotropic model over a spherical geodesic grid. Truncation error considerations show that the grid resolution must be at least as fine as $2\frac{1}{2}°$ in order for the error not to dominate the mass flux calculations. When the fine resolution is used, the approximations are seen to be quite good. Comparisons are made with schemes in use today with approximately the same resolution applied to the same initial condition.

1. INTRODUCTION

In recent years, numerical experimenters have been studying models of the general circulation of the atmosphere over the entire earth. The use of a spherical domain has led to the unexpected difficulty of defining a satisfactory net of points at which discrete approximations are to be applied. Many schemes have been suggested and tried, but all have some unfavorable property.

A homogeneous covering of the sphere seems to be ideal for numerical integration. However, a completely homogeneous net is impossible if it consists of more than 12 points. Quasi-homogeneous triangular grids have been defined over the sphere by Vestine et al. (1963), Sadourny et al. (1968), and Williamson (1968). Sadourny et al. (1968) and Williamson (1968) have developed and tested discrete approximations for the nondivergent barotropic vorticity equation over these grids. Their results are more favorable than those of the more usual spherical grids in use today.

In the following report, conservative approximations over the spherical geodesic grid are developed and tested for the primitive barotropic model. This spherical development closely follows the development in Cartesian geometry (Williamson 1969).

Let **i**, **j**, and **k** be unit vectors on the sphere in the eastward, northward, and vertical directions, respectively; and let ∇ be the spherical horizontal gradient operator. Then the equations governing frictionless, horizontal, two-dimensional motion on a sphere can be written

$$\frac{\partial h\mathbf{V}}{\partial t} = -\nabla \cdot (\mathbf{V}h\mathbf{V}) - \mathbf{F} \times h\mathbf{V} - \nabla(gh^2/2) \quad (1)$$

and

$$\frac{\partial h}{\partial t} = -\nabla \cdot (h\mathbf{V}) \quad (2)$$

where h is the height of the free surface, $\mathbf{V} = u\mathbf{i} + v\mathbf{j}$ is the vector velocity, and $\mathbf{F}$ equals $(f + (u/a) \tan \theta)\mathbf{k}$. The a is

[1] Previous affiliation, Department of Meteorology, Massachusetts Institute of Technology, Cambridge, Mass.

[2] The National Center for Atmospheric Research is sponsored by the National Science Foundation.

the radius of the sphere, f is the Coriolis parameter, θ is the latitude, and g is gravity.

2. CONSERVATIVE APPROXIMATIONS

The discrete approximations are based on area integrals over the secondary grid areas defined by the perpendicular bisectors of the grid triangle sides. The integrals of the divergence can be converted to line integrals using Gauss' Theorem, resulting in

$$\frac{\partial}{\partial t} \int_A h\mathbf{V}dA = -\oint_S (\mathbf{V}h\mathbf{V}) \cdot \mathbf{n}dS -$$
$$g\int_A \nabla \frac{h^2}{2} dA - \int_A \mathbf{F} \times h\mathbf{V}dA \quad (3)$$

and

$$\frac{\partial}{\partial t} \int_A hdA = -\oint_S (\mathbf{V}h) \cdot \mathbf{n}dS \quad (4)$$

where **n** is the outward unit normal to the curve S bounding the area A.

A local polar indexing is used to write the difference equations (Williamson 1969). Let k denote the number of triangles surrounding the grid point in question. For the spherical geodesic grid, k is either five or six. Consider first a general form of approximation to the divergence of some vector quantity **B**:

$$D = \oint_S \mathbf{B} \cdot \mathbf{n}dS.$$

If we assume the value of **B** along the ith segment S_i of S is constant and given by $\mathbf{B}_{1/2, i}$, the approximation to the divergence becomes

$$D \doteq \sum_{i=1}^{k} \mathbf{B}_{1/2, i} \cdot \int_{S_i} \mathbf{n}dS \quad (5)$$

where S_i denotes the great circle segments forming the secondary grid area. By the line integral of the unit normal vector, we mean the line integral of the two components of the unit normal written in spherical polar coordinates. It is easy to show that many approximations

used in calculating fluid flow a.e of the general form of equation (5). For a grid of the kind used by Washington and Kasahara (1970), the line integrals of the components reduce to the very simple forms $\pm$ i$\Delta\theta$, or $\pm$ j$\Delta\lambda$. In the case of the grid developed by Kurihara, they take the form (in Gary's 1969 notation) of $\pm$ iS_m, or $\pm$ jS_m. The line integrals of the normal components in the spherical geodesic grid do not reduce to anything quite so simple. In fact, the expressions for the integrals along arbitrary great circle grid segments are difficult to calculate analytically. In this study, they are calculated numerically. It should be pointed out that the coefficients can be calculated with a very high degree of precision since they need be calculated only once for each grid orientation and resolution. We denote these line integrals by $\vec{C}_i$, that is,

$$\vec{C}_i = \int_{S_i} \mathbf{n} dS. \tag{6}$$

We now consider an approximation to the pressure gradient term

$$G = \int_A \nabla h dA.$$

Written in spherical coordinates, the integral becomes

$$G = \int_A \int \left[\frac{1}{a \cos\theta} \frac{\partial h}{\partial\lambda} \mathbf{i} + \frac{1}{a} \frac{\partial h}{\partial\theta} \mathbf{j} \right] a^2 \cos\theta d\theta d\lambda$$

or

$$G = \int_A \int \left[a \frac{\partial h}{\partial\lambda} \mathbf{i} + a \frac{\partial(h \cos\theta)}{\partial\theta} \mathbf{j} \right] d\theta d\lambda + \int_A \int ah \sin\theta \mathbf{j} d\theta d\lambda.$$

After neglecting the spatial variation of the unit vectors within the secondary grid area, the first integral on the right-hand side can be shown to be a line integral of h times the outward unit normal and can be approximated by

$$\sum_{i=1}^{k} (h)_{1/2,i} \vec{C}_i. \tag{7}$$

If, in addition, the variation of h in the secondary grid area is neglected, the second term on the right-hand side becomes

$$-h^* \int_\lambda a \cos\theta \Big|_{\theta_1(\lambda)}^{\theta_2(\lambda)} \mathbf{j} d\lambda$$

where h^* denotes some average value of h. This integral can be written approximately as

$$-\sum_{i=1}^{k} h^*(\vec{C}_i \cdot \mathbf{j})\mathbf{j}. \tag{8}$$

Terms (7) and (8) can be combined for an approximation to the pressure gradient

$$G \doteq \sum_{i=1}^{k} (h)_{1/2,i} \vec{C}_i - \sum_{i=1}^{k} h^*(\vec{C}_i \cdot \mathbf{j})\mathbf{j}. \tag{9}$$

We are now able to write a general approximation to equations (3) and (4). Using the approximations (5) and (9), the governing equations become

$$A_0 \frac{\partial h_0 \mathbf{V}_0}{\partial t} = -\sum_{i=1}^{k} (\mathbf{V}h\mathbf{V})_{1/2,i} \cdot \vec{C}_i - g \sum_{i=1}^{k} \left(\frac{h^2}{2}\right)_{1/2,i} \vec{C}_i$$
$$+ g \sum_{i=1}^{k} \left(\frac{h^2}{2}\right)^* (\vec{C}_i \cdot \mathbf{j})\mathbf{j} - A_0 \mathbf{F}_0 \times h_0 \mathbf{V}_0 \tag{10}$$

and

$$A_0 \frac{\partial h_0}{\partial t} = -\sum_{i=1}^{k} (h\mathbf{V})_{1/2,i} \cdot \vec{C}_i. \tag{11}$$

Let $\bar{\psi}$ denote the finite-difference equivalent to integration of a quantity ψ over the sphere, that is,

$$\bar{\psi} = \frac{1}{A_s} \Sigma A_0 \psi_0$$

where the summation is taken over all grid points and A_s is the area of the sphere.

Formation of the discrete energy equation shows that for (10) and (11) to conserve energy, the following relations must hold

$$\overline{\tfrac{1}{2}\mathbf{V}_0^2 \sum_{i=1}^{k} (\mathbf{V}h)_{1/2,i} \cdot \vec{C}_i} = \overline{\mathbf{V}_0 \cdot \sum_{i=1}^{k} (\mathbf{V}h\mathbf{V})_{1/2,i} \cdot \vec{C}_i} \tag{12}$$

and

$$\overline{\mathbf{V}_0 \cdot \sum_{i=1}^{k} \left(\frac{h^2}{2}\right)_{1/2,i} \vec{C}_i - \mathbf{V}_0 \cdot \sum_{i=1}^{k} \left(\frac{h^2}{2}\right)^* (\vec{C}_i \cdot \mathbf{j})\mathbf{j}}$$
$$= -\overline{h_0 \sum_{i=1}^{k} (\mathbf{V}h)_{1/2,i} \cdot \vec{C}_i}. \tag{13}$$

The first relation (12) insures that the space differences will not produce nonlinear instabilities; the second relation (13) provides for consistent average conversion between kinetic and potential energy.

We note that when the curvilinear coordinate system reduces to the Cartesian system, equations (10) through (13) reduce to the corresponding Cartesian equations (10) through (13) in Williamson (1969).

Relation (12) can be satisfied if we take

$$(\mathbf{V}h\mathbf{V})_{1/2,i} = \tfrac{1}{2}(\mathbf{V}_0 + \mathbf{V}_{1,i})(\mathbf{V}h)_{1/2,i} \tag{14}$$

since, as in the Cartesian case,

$$\overline{\sum_{i=1}^{k} \mathbf{V}_0 \cdot \mathbf{V}_i (\mathbf{V}h)_{1/2,i} \cdot \vec{C}_i} = 0.$$

One possible definition of $(\mathbf{V}h)_{1/2,i}$ is

$$(\mathbf{V}h)_{1/2,i} = \tfrac{1}{2}(h_0 \mathbf{V}_0 + h_i \mathbf{V}_i). \tag{15}$$

The energy conversion relation (13) then holds provided that

$$(h^2)_{1/2,i} = h_0 h_i \tag{16}$$

and

$$(h^2)^* = h_0^2. \tag{17}$$

Substitution of (14), (15), (16), and (17) into (10) and (11) results in *scheme I*s:

$$\frac{\partial h_0 \mathbf{V}_0}{\partial t} = -\frac{1}{4A_0} \sum_{i=1}^{k} (\mathbf{V}_0 + \mathbf{V}_i)(h_0 \mathbf{V}_0 + h_i \mathbf{V}_i) \cdot \vec{C}_i$$

$$-\frac{g}{2A_0} \sum_{i=1}^{k} h_0 h_i \vec{C}_i + \frac{g}{2A_0} h_0^2 \sum_{i=1}^{k} (\vec{C}_i \cdot \mathbf{j}) \mathbf{j} - \mathbf{F}_0 \times h_0 \mathbf{V}_0$$

and

$$\frac{\partial h_0}{\partial t} = -\frac{1}{2A_0} \sum_{i=1}^{k} (h_0 \mathbf{V}_0 + h_i \mathbf{V}_i) \cdot \vec{C}_i.$$

The special form this scheme takes when applied to a regular spherical grid is the same as the scheme of Grimmer and Shaw (1967).

A second possible definition of $(\mathbf{V}h)_{1/2,\,i}$ is

$$(\mathbf{V}h)_{1/2,\,i} = \tfrac{1}{4}(h_0 + h_i)(\mathbf{V}_0 + \mathbf{V}_i). \tag{18}$$

Relation (13) is now valid if

$$(h^2)_{1/2,\,i} = \tfrac{1}{2}(h_0^2 + h_i^2) \tag{19}$$

and

$$(h^2)^* = h_0^2. \tag{20}$$

Substitution of (14), (18), (19), and (20) into (10) and (11) results in a second energy conservative scheme given by *scheme II*s:

$$\frac{\partial h_0 \mathbf{V}_0}{\partial t} = -\frac{1}{8A_0} \sum_{i=1}^{k} (\mathbf{V}_0 + \mathbf{V}_i)(h_0 + h_i)(\mathbf{V}_0 + \mathbf{V}_i) \cdot \vec{C}_i$$

$$-\frac{g}{4A_0} \sum_{i=1}^{k} (h_0^2 + h_i^2) \vec{C}_i + \frac{g}{2A_0} h_0^2 \sum_{i=1}^{k} (\vec{C}_i \cdot \mathbf{j}) \mathbf{j} - \mathbf{F}_0 \times h_0 \mathbf{V}_0$$

and

$$\frac{\partial h_0}{\partial t} = -\frac{1}{4A_0} \sum_{i=1}^{k} (h_0 + h_i)(\mathbf{V}_0 + \mathbf{V}_i) \cdot \vec{C}_i.$$

The special form which scheme IIs takes when applied to a regular spherical grid is the same as Kurihara's scheme as studied by Gary (1969).

3. NUMERICAL EXPERIMENTS

To evaluate these schemes for use with atmospheric-like motions, we adopt the initial conditions used by Phillips (1959) and subsequently by other investigators. These conditions are those of a Neamtan (1946) wave that, in a nondivergent barotropic atmosphere, propagates eastward with a constant angular velocity and without change of shape. The analytic solution is not known for the divergent model considered here. However, several investigators, namely Grimmer and Shaw (1967) and Gary (1969), have used these same initial conditions to test difference approximations for the same model. Our results can be compared with theirs, and hence the difference schemes can be compared with each other. These initial conditions have another advantage; since they are analytic, the exact initial fluxes can be calculated and compared with the discrete initial fluxes.

For the following integrations, the spherical geodesic grid is oriented so that the North and South Poles are grid points (fig. 4, Williamson 1968). This orientation is useful for our evaluation run because the grid then has a period of five around the sphere. If the initial conditions also have a period of five, only one-fifth of the computations need to be performed. Our experiments take advantage of this feature.

This orientation is not desirable for general usage, since the Poles must be treated separately when spherical polar coordinates are used. In this case, the velocity components u and v are not defined at the Poles. Since there is little happening at the Poles with the Neamtan wave, the velocity $\mathbf{V}$ is set equal to zero, and the height h is assigned the average value of the five closest points when these polar values are needed by the difference operators.

The initial velocity $\mathbf{V}$ is nondivergent and given by the stream function

$$\psi = -a^2 \omega \sin \theta + a^2 K \cos^R \theta \sin \theta \cos R\lambda$$

where a is the earth's radius, ω and K are 7.848×10^{-6} sec^{-1}, and R is taken equal to 5 rather than 4, which Phillips (1959) used. The initial height field is taken so that h and ψ satisfy the balance equation, and is given by equation (38) in Phillips (1959).

A 6-day (6,912-time step) integration with a 75-sec time step was carried out over the 5° grid using centered time differences. A forward time step was used initially. Figure 1 shows the height field at 2-day intervals. The region covered by each figure is −90° to +90° latitude and 0° to 150° longitude, a little over two periods. The wave speed is slightly over 17° per day compared with an analytic value for the nondivergent case of 19.8. The fields become very jagged, and the solution is not good at day 6.

Figure 1 also shows the results of an 8-day (18,432-time step) integration with 37.5-sec time step over a 2½° grid using centered time steps. The most noticeable feature is the two-grid-interval noise superimposed on the pattern. Such phenomena are present in other schemes (Okamura 1969) and can be avoided by changing the space phasing of the variables (Masuda 1969, Okamura 1969) or by adding a diffusion term or space smoothing.

Disregarding this two-grid-interval noise, these results can be smoothed by eye and compared with previous investigations. For the first 4 or 5 days, when the original wave is still clearly defined in the pattern, the wave moved with a speed slightly greater than 18° per day. Again, the analytic value for the nondivergent model is about 19.8.

Gary (1969) compared two schemes currently being used for general circulation models: Kurihara's (1965b) and Kasahara and Washington's (1967), hereafter referred to as "centered." Gary concluded that the Kurihara scheme is more accurate than the centered scheme for a given $\Delta\theta$. However, because of the space-time phasing of the variables, Gary feels the Kurihara scheme at $\Delta\theta$ should be compared with the centered scheme at approxi-
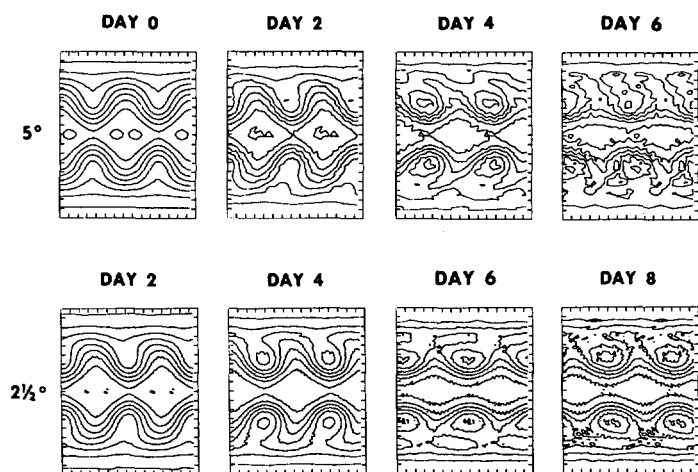
FIGURE 1.—Height field from 5° and 2½° integrations using scheme IIs with centered time differences.

mately $\Delta\theta/\sqrt{2}$. Further information he gives suggests that under these conditions the schemes are probably equally good. Gary also concluded that the Kurihara scheme with a "uniform mesh" spacing, in which the number of grid points on a latitude circle decreases uniformly from Equator to Pole, produces less accurate results than one in which $\Delta\lambda$ was constant and equal to $\Delta\theta$ up to around $\theta=65°$ and then increased.

Recent experiments by Dey (1969) and Rao and Umscheid (1969) show that marked improvements in the integrations result when the longitudinal grid spacing near the Pole is decreased. However, such a decrease inflicts a serious decrease on the time step through linear stability. Dey decreased his time step by a factor of 3, and Rao and Umscheid decreased theirs by a factor of 10.

With this in mind, we will compare our results with those of the Kurihara scheme over a regular spherical mesh, not the uniform mesh as originally defined by Kurihara (1965b). We will consider the case where the resolution at the Equator is approximately equal to ours. This is Gary's case 503.1 or his figure 8. This case has a grid size of about 2.65° at the Equator with the resolution increasing up to about 65° latitude. This grid has 7,044 points compared with 7,682 points in the 2½° spherical geodesic grid.

Our patterns evolved very closely to those of Kurihara's scheme. The main difference is that by the eighth day his patterns become weak, due to a diffusion term added for stability. Essentially, these schemes produce very similar results for this type of initial condition, and we conclude that in this respect the schemes are equally good.

We can also compare our results to Gary's figure 9, which is the solution from Kurihara's scheme applied to his uniform grid. Our results are seen to be better than these.

We cannot compare the energy conservation properties of these schemes since Gary always used a diffusion term for stability. Hence the energy in his cases always decreased. The total energy per unit area in our 2½° integration remained in the range 4.61564×10^8 to $4.61588 \times$

10^8 during the entire 8 days. The energy variation in the 5° integration was of the same order, about 0.003 percent.

From these comparisons, we conclude that the space differences over the spherical geodesic grid are at least as good as those in use today for general circulation models when applied to a simple wave. However, when the spherical geodesic schemes are combined with centered time differencing, a very small time step is required for linear stability. One of the reasons for using a quasi-homogeneous grid is to eliminate the convergence of grid points at the Pole and the very small time step this convergence imposes. It is not known why these schemes coupled with centered time steps required such a small time step. The linear stability condition is difficult to compute because the coefficients of the finite-difference approximations are different for each grid point and are not known analytically. The time step needed to keep these schemes stable is an order of magnitude smaller than stability limit for simple schemes centered in space and time.

The Matsuno, or Euler-backward time differencing (Kurihara 1965a), was tried to determine the effect of a damping scheme on the approximations. A 20-min time step was found to be stable for the 5° grid, and a 10-min step for the 2½° grid. This is more consistent with the normal linear stability criterion and is up to four times longer than would be necessary for the present general circulation models at a similar resolution. Time steps that have been used are: Mintz (1965), $\Delta t=12$ min for $\Delta\theta=7°$; Kasahara and Washington (1969), $\Delta t=6$ min for $\Delta\theta=5°$; and Kurihara and Holloway (1967), $\Delta t=7.5$ min for $\Delta\theta=4°$.

Height fields for various days are shown in figure 2 for the 5° and 2½° grid using Matsuno time differences. The time steps used are 20 min and 7.5 min for the 5° and 2½° grids, respectively. With a 10-min time step on the 2½° grid, a two-grid-interval wiggle appeared in limited areas at various times and then disappeared. No sign of this phenomenon was seen with the 7.5-min time step. Figure 2 can be compared with figure 1. The height field patterns are very similar. The Matsuno scheme produces a slightly slower phase speed than the centered scheme. The Matsuno scheme also produces a slight damping. The total energy decreased by 0.4 percent during the 8-day run over the 2½° grid. Other than these slight differences, the same conclusions can be made for the spherical geodesic differences combined with the Matsuno scheme as were made when they were combined with the centered scheme.

4. FLUX APPROXIMATIONS

To better understand how these schemes work, we consider the initial flux approximations. The analytic initial conditions permit the initial fluxes to be calculated analytically and compared with the discrete fluxes. This will help explain why the 5° grid produced poor results. First, it will prove useful to introduce another approximation to the mass flux.
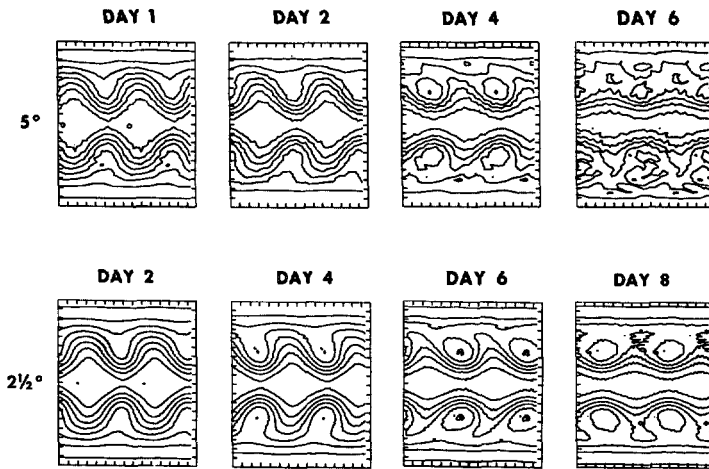
FIGURE 2.—Height field from 5° and 2½° integrations using scheme IIs with Matsuno time differences.

The mass flux can be written as the sum of an advection and a divergence term

$$\nabla \cdot (h\mathbf{V}) = \mathbf{V} \cdot \nabla h + h\nabla \cdot \mathbf{V},$$

and each term can be differenced independently. From (9) and (5) we have approximations for ∇h and $\nabla \cdot \mathbf{V}$, namely

$$\nabla \cdot \mathbf{V} = \frac{1}{A_0} \sum_{i=1}^{k} \tfrac{1}{2}(\mathbf{V}_0 + \mathbf{V}_i) \cdot \vec{C}_i$$

and

$$\nabla h = \frac{1}{2A_0} \sum_{i=1}^{k} (h_i - h_0)\vec{C}_i.$$

Thus, we can write an approximation IIIs as scheme IIIs:

$$\mathbf{V} \cdot \nabla h = \frac{\mathbf{V}_0}{2A_0} \cdot \sum_{i=1}^{k} (h_i - h_0)\vec{C}_i,$$

$$h\nabla \cdot \mathbf{V} = \frac{h_0}{2A_0} \sum_{i=1}^{k} (\mathbf{V}_i + \mathbf{V}_0) \cdot \vec{C}_i,$$

and

$$\nabla \cdot (h\mathbf{V}) = \frac{1}{2A_0} \sum_{i=1}^{k} (\mathbf{V}_0 h_i + \mathbf{V}_i h_0) \cdot \vec{C}_i.$$

This approximation has the same general form as Is and IIs, and, as will be seen, gives very similar results. To study the initial fluxes, we use a wave-number-4 initial condition rather than a wave number 5. This prevents the grid pattern and wave pattern from coinciding.

The left column of figure 3 shows the initial analytic flux fields. The two other columns show the flux fields as calculated by scheme IIs over a 10° and 5° grid. The momentum fluxes are seen to be quite good, but the mass flux only begins to resemble the analytic field with the 5° grid. The pressure gradient approximations, not shown, are at least as good as the momentum flux approximations. Thus, we will confine the ensuing discussion to the momentum and mass flux. The question we wish to con-

sider is why the mass flux approximations are so much poorer than the momentum fluxes.

Figure 4 shows the approximations of scheme IIIs for the 10° and 5° grids. The mass flux is almost identical with that from scheme IIs. Of the two individual parts of the mass flux, the advection term is a good approximation to the mass flux, but the divergence term, which should be zero, is poor. In fact, the approximation values of the divergence are larger than the mass flux for the 10° grid and almost as large for the 5° grid. Examination of the truncation error will explain why the divergence approximation is so poor.

5. TRUNCATION ERROR

To study the truncation error, we apply the difference scheme over a stencil of points more naturally suited to polar spherical coordinates. Consider four grid points around a central point such that two have the same latitude as the central point and two have the same longitude, although they need not be the same distance from the central point (fig. 5). To apply the schemes to this stencil, we need the line integrals of the normal vectors and the area. These are given by

$$\vec{C}_1 = a\Delta\theta^* \mathbf{i},$$

$$\vec{C}_2 = a \cos\left(\theta_0^* + \frac{\Delta\theta^*}{2}\right)\Delta\lambda^* \mathbf{j},$$

$$\vec{C}_3 = -a\Delta\theta^* \mathbf{i},$$

$$\vec{C}_4 = -a \cos\left(\theta_0^* - \frac{\Delta\theta^*}{2}\right)\Delta\lambda^* \mathbf{j},$$

and

$$A_0 = 2a^2 \sin\frac{\Delta\theta^*}{2} \cos\theta_0^*\Delta\lambda^*$$

where

$$\Delta\lambda^* = \tfrac{1}{2}(\Delta\lambda_1 + \Delta\lambda_3),$$

$$\Delta\theta^* = \tfrac{1}{2}(\Delta\theta_2 + \Delta\theta_4),$$

and

$$\theta_0^* = \theta_0 + \tfrac{1}{4}(\Delta\theta_2 - \Delta\theta_4).$$

In the following, approximations over two cases of this stencil are considered. The first case is called *regular spherical differences*. At each grid point of the 5° spherical geodesic grid, the stencil is defined so that $\Delta\lambda_1 = \Delta\lambda_3 = \Delta\theta_2 = \Delta\theta_4 = D$. At each of these newly defined stencil points, the appropriate analytic values are assigned to h, u, and v. The difference schemes are applied over this new stencil. We note that this is *not* appropriate for integrating in time, but rather is only appropriate for studying the approximations to the intital fluxes.

The second case considered is called *random spherical differences*. In this case $\Delta\lambda_1$, $\Delta\lambda_3$, $\Delta\theta_2$, and $\Delta\theta_4$ are given by $D(1.0 + 0.1R)$ where D is the mean value and R is a random number between -1 and $+1$ with a rectangular
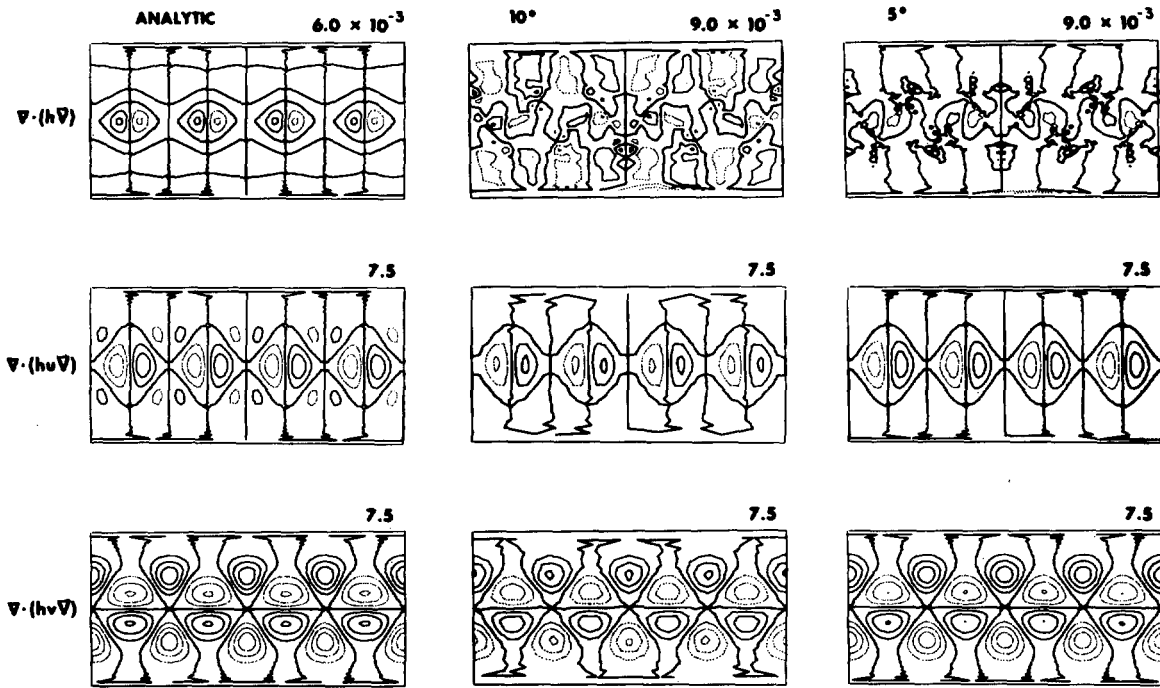
FIGURE 3.—Initial analytic fluxes and scheme Is approximations over 10° and 5° grids. The contour intervals are given in the upper right corners.

distribution. A 10 percent variation was chosen to correspond to the variation in the grid length of the spherical geodesic grid. In the following, we will refer to 10°, 5° and 2½° stencils. This indicates the value of D for both the regular and random stencils.

We first consider the truncation error over the random spherical stencil. Schemes Is and IIs produce almost identical results. Therefore, since scheme Is is a little simpler, we will consider it in the following. The terms considered are:

scheme Is, momentum flux

$$Q_1 = -\frac{1}{4A_0} \sum_{i=1}^{k} (\mathbf{V}_0 + \mathbf{V}_i)(h_0\mathbf{V}_0 + h_i\mathbf{V}_i) \cdot \vec{C}_i;$$

scheme Is, mass flux

$$M_1 = -\frac{1}{2A_0} \sum_{i=1}^{k} (h_0\mathbf{V}_0 + h_i\mathbf{V}_i) \cdot \vec{C}_i;$$

scheme IIIs, advection term

$$A_2 = -\frac{1}{2A_0} \sum_{i=1}^{k} \mathbf{V}_0(h_i - h_0) \cdot \vec{C}_i;$$

scheme IIIs, divergence term

$$D_2 = -\frac{1}{2A_0} \sum_{i=1}^{k} h_0(\mathbf{V}_0 + \mathbf{V}_i) \cdot \vec{C}_i;$$

and
scheme IIIs, mass flux

$$M_2 = A_2 + D_2 = -\frac{1}{2A_0} \sum_{i=1}^{k} (h_i\mathbf{V}_0 + h_0\mathbf{V}_i) \cdot \vec{C}_i.$$

The quantities in the difference approximations are expanded in Taylor series around the center point

$$\psi_i = \psi_0 + \sum_{j=1}^{\infty} \frac{1}{j!} \Delta\lambda_i^j \frac{\partial^j\psi_0}{\partial\lambda^j}, \text{ for } \psi=\mathbf{V} \text{ or } h \text{ and } i=1 \text{ or } 3,$$

and

$$\psi_i = \psi_0 + \sum_{j=1}^{\infty} \frac{1}{j!} \Delta\theta_i^j \frac{\partial^j\psi_0}{\partial\theta^j}, \text{ for } \psi=\mathbf{V} \text{ or } h \text{ and } i=2 \text{ or } 4.$$

The following simplifications are made in the expansions

$$4 \sin \frac{\Delta\theta_2 + \Delta\theta_4}{4} \doteq \Delta\theta_2 + \Delta\theta_4$$

and

$$\cos \frac{\Delta\theta_2 + \Delta\theta_4}{2} \doteq 1.$$

These simplifications affect the results by less than 1 percent, *not* by orders of magnitude.

The Taylor series expansions for the approximations are then

$$\vec{Q}_1 = -\nabla \cdot (\mathbf{V}h\mathbf{V}) - \delta\lambda\vec{Q}_{1\lambda} - \delta\theta\vec{Q}_{1\theta} + 0(\Delta^2),$$

$$M_1 = -\nabla \cdot (h\mathbf{V}) - \delta\lambda M_{1\lambda} - \delta\theta M_{1\theta} + 0(\Delta^2),$$

$$A_2 = -\mathbf{V} \cdot \nabla h - \delta\lambda A_{2\lambda} - \delta\theta A_{2\theta} + 0(\Delta^2),$$

and

$$D_2 = -h\nabla \cdot \mathbf{V} - \delta\lambda D_{2\lambda} - \delta\theta D_{2\theta} + 0(\Delta^2)$$

where

$$\delta\theta = \frac{(\Delta\theta_2 - \Delta\theta_4)}{2},$$

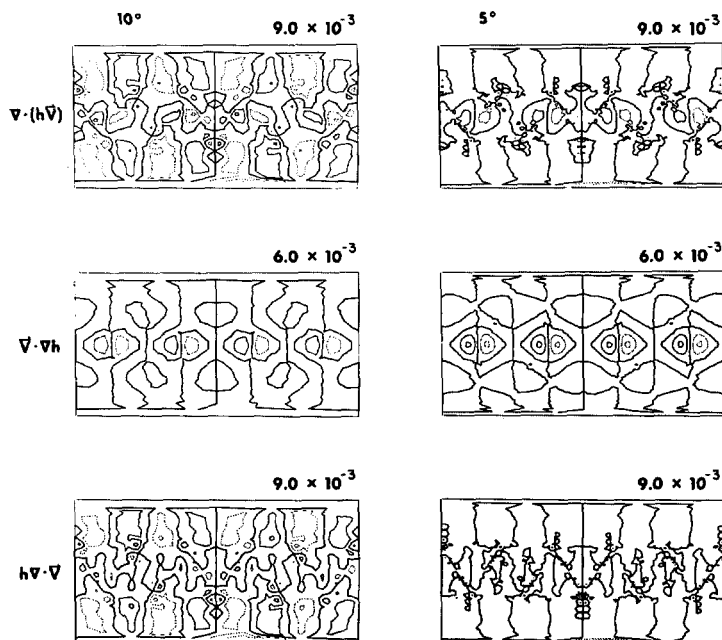$$\delta\lambda = \frac{(\Delta\lambda_1 - \Delta\lambda_3)}{2},$$

FIGURE 4.—Scheme IIIs approximations over 10° and 5° grids. The contour intervals are given in the upper right corners.

FIGURE 5.—Random stencil.

$$\vec{Q}_{1\lambda}=\frac{1}{2a\cos\theta}\left\{hu\frac{\partial^2\mathbf{V}}{\partial\lambda^2}+\mathbf{V}\frac{\partial^2 hu}{\partial\lambda^2}+\frac{\partial^2}{\partial\lambda^2}(hu\mathbf{V})\right\},$$

$$\vec{Q}_{1\theta}=\frac{1}{a}\left\{hv\frac{\partial^2\mathbf{V}}{\partial\theta^2}+\mathbf{V}\frac{\partial^2 hv}{\partial\theta^2}+\frac{\partial^2}{\partial\theta^2}(hv\mathbf{V})-2\tan\theta\frac{\partial}{\partial\theta}(hv\mathbf{V})\right\},$$

$$M_{1\lambda}=\frac{1}{a\cos\theta}\frac{\partial^2}{\partial\lambda^2}(hu),$$

$$M_{1\theta}=\frac{1}{a}\left\{\frac{\partial^2}{\partial\theta^2}(hv)-\frac{\tan\theta}{2}\frac{\partial}{\partial\theta}(hv)\right\},$$

$$A_{2\lambda}=\frac{u}{a\cos\theta}\frac{\partial^2 h}{\partial\lambda^2},$$

$$A_{2\theta}=\frac{v}{a}\left\{\frac{\partial^2 h}{\partial\theta^2}-\frac{\tan\theta}{2}\frac{\partial h}{\partial\theta}\right\},$$

$$D_{2\lambda}=\frac{h}{a\cos\theta}\frac{\partial^2 u}{\partial\lambda^2},$$

and

$$D_{2\theta}=\frac{h}{a}\left\{\frac{\partial^2 v}{\partial\theta^2}-\frac{\tan\theta}{2}\frac{\partial v}{\partial\theta}\right\}.$$

The second column in table 1 gives the maximum absolute value of the above terms for wave number 5. With the random stencil defined earlier, $|(\Delta\lambda_1-\Delta\lambda_3)/2|$ and $|(\Delta\theta_2-\Delta\theta_4)/2|$ are less than $0.1\Delta\lambda^*$ and $0.1\Delta\theta^*$, respectively. Thus, the maximum value of the truncation error for the advection term of scheme IIIs is bounded by $0.1\Delta\lambda^*|A_{2\lambda}|$ or $0.1\Delta\theta^*|A_{2\theta}|$, and similarly for the other terms. These error bounds are listed in table 1. For comparison, the right side of the table lists the maximum absolute values of the momentum and mass fluxes and the advection terms for wave number 5.
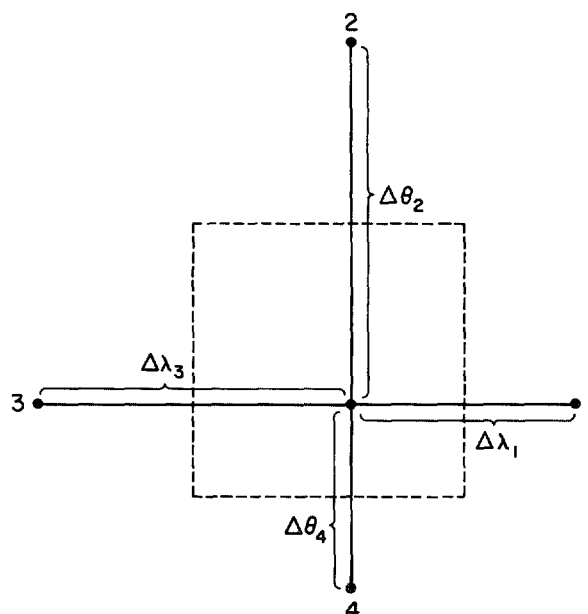
Comparison shows that the maximum possible errors in the monentum flux approximations are less than the analytic values even for the 10° stencil and are at least an order of magnitude smaller for the 2½° stencil. This is not the case for the mass flux. Here, the maximum possible errors are the same size as the mass flux even with the 5° grid. Examination of scheme IIIs in the table shows this error can be attributed to the error in the divergence term. The error in the divergence does not adversely affect the momentum flux because the momentum flux is three orders of magnitude larger than the mass flux. But since $hu\nabla\cdot\mathbf{V}=u(h\nabla\cdot\mathbf{V})$ and u is less than 100 m sec^{-1}, if the error in the divergence term is the same order as the advection term in the mass flux, the error in the divergence term is at least one order smaller than the momentum flux.

Table 1 lists error bounds and compares them with the analytic values of the continuous terms. Of course, the actual errors are not necessarily as large as the bounds.

Actual computations over the random stencils show that the errors are significant for the 10° and 5° random stencils. The patterns of the mass flux are as irregular as those over the spherical geodesic grid. The mass flux begins to resemble the actual values with the 2½° stencil; however, the contour lines are still quite ragged as in figure 4. On the other hand, the momentum fluxes over the random stencils are quite good, even for the 10° stencil.

When these schemes are applied to the regular stencil, the first-order error term automatically becomes zero. Computations over the regular stencil show that the errors in the mass flux become negligible even for the 5° stencil. A contour of the mass flux over the 2½° regular stencil is almost the same as the analytic values in figure 3.

The above error studies show that the small irregularities of the spherical geodesic grid make the usual type

TABLE 1.—*Error bounds for random stencil*

Term	Maximum absolute value	10°	5°	2½°	Maximum absolute value	Term
$\vec{Q}_{1\lambda}\cdot i$	3.9×10²	6.8×10⁰	3.4×10⁰	1.7×10⁰	2.4×10¹	∇·(Vhu)
$\vec{Q}_{1\theta}\cdot i$	9.4×10¹	1.7×10⁰	8.2×10⁻¹	4.1×10⁻¹		
$\vec{Q}_{1\lambda}\cdot j$	1.2×10³	2.1×10¹	1.1×10¹	5.3×10⁰	3.4×10¹	∇·(Vhv)
$\vec{Q}_{1\theta}\cdot j$	1.6×10²	2.8×10⁰	1.4×10⁰	7.0×10⁻¹		
$M_{1\lambda}$	2.0×10⁰	3.7×10⁻²	1.9×10⁻²	9.2×10⁻³	1.3×10⁻²	∇·hV
$M_{1\theta}$	1.3×10⁰	2.3×10⁻²	1.2×10⁻²	5.7×10⁻³		
$A_{2\lambda}$	1.9×10⁻¹	3.3×10⁻³	1.7×10⁻³	8.3×10⁻⁴	1.3×10⁻²	∇·∇h
$A_{2\theta}$	8.6×10⁻²	1.5×10⁻³	7.5×10⁻⁴	3.8×10⁻⁴		
$D_{2\lambda}$	2.1×10⁰	3.7×10⁻³	1.9×10⁻³	9.2×10⁻³	0	h∇·V
$D_{2\theta}$	1.3×10⁰	2.3×10⁻²	1.2×10⁻²	5.7×10⁻³		

of conservative approximations first order in space. This first-order error can be quite important in calculating the mass flux. It is not until the grid resolution is as fine as 2½° that the error becomes small enough to perform integrations in time.

6. CONCLUSIONS

In an earlier paper (Williamson 1968), a spherical geodesic grid was introduced. Such a grid is quasi-homogeneous with about a 10 percent variation in the grid interval. Difference approximations were formulated for the nondivergent barotropic vorticity equation. Test integrations showed that this model worked quite well over this grid.

The primitive model formulated in this paper shows that the small variation in grid interval does introduce an unexpected problem. Conservative difference schemes that are second order when applied to a regular grid become first order when applied to a nonregular grid. In the models considered, the first-order error is significant only in calculating the divergence. As was mentioned earlier, there is no trouble in integrating the nondivergent barotropic vorticity equation. For the primitive model with a Neamtan wave initial condition, the error can be significant. This is seen in the integration over a 5° grid.

The truncation error can be made insignificant by taking a fine-enough mesh. This is seen with the 2½° integration. The need for a fine mesh for a satisfactory approximation is not necessarily a handicap. Studies by Grammeltvedt (1969) and Gary (1969) indicate that at least 16 points per wavelength are needed for a satisfactory approximation to the phase velocity even with second- and fourth-order schemes. Thus, the 2½° grid is suitable up to wave number 9. An even finer grid is needed for smaller waves.

Once the mesh size is small enough, the spherical geodesic schemes are seen to produce good results. Compared to Kurihara's scheme over his uniform grid, the spherical geodesic schemes are seen to be much better. On the other hand, the spherical geodesic schemes produce the same

results as the Kurihara scheme over a regular spherical grid. The spherical geodesic schemes are also slightly better than the scheme of Kasahara and Washington.

The particular time differencing combined with the spherical geodesic differences is important. Centered time differences produce very good results, especially with regard to energy conservation. However, a very small time step is needed for stability. In fact, the time step must be almost as small as would be needed with a regular spherical grid if there were no skipping of grid points near the Poles.

The Matsuno time difference, on the other hand, remains stable for a much larger time step. A time step up to four times longer than the time steps of the other spherical schemes is possible. Depending on the complexity of the other schemes, this could mean a savings of four in computer time. A more realistic figure is a little less than three because the spherical geodesic schemes use six surrounding points rather than the more normal four.

REFERENCES

Dey, Clifford H., "A Note on Global Forecasting With the Kurihara Grid," *Monthly Weather Review*, Vol. 97, No. 8, Aug. 1969, pp. 597–601.

Gary, J. M., "A Comparison of Difference Schemes Used for Numerical Weather Prediction," *Journal of Computational Physics*, Vol. 4, No. 3, Oct. 1969, pp. 279–305.

Grammeltvedt, Arne, "A Survey of Finite-Difference Schemes for the Primitive Equations for a Barotropic Fluid," *Monthly Weather Review*, Vol. 97, No. 5, May 1969, pp. 384–404.

Grimmer, M., and Shaw, D. B., "Energy-Preserving Integrations of the Primitive Equations on the Sphere," *Quarterly Journal of the Royal Meteorological Society*, Vol. 93, No. 397, July 1967, pp. 337–349.

Kasahara, Akira, and Washington, Warren M., "NCAR Global General Circulation Model of the Atmosphere," *Monthly Weather Review*, Vol. 95, No. 7, July 1967, pp. 389–402.

Kurihara, Yoshio, "On the Use of Implicit and Iterative Methods for the Time Integration of the Wave Equation," *Monthly Weather Review*, Vol. 93, No. 1, Jan. 1965a, pp. 33–46.

Kurihara, Yoshio, "Numerical Integration of the Primitive Equations on a Spherical Grid," *Monthly Weather Review*, Vol. 93, No. 7 July 1965b, pp. 399–415.

Kurihara, Yoshio, and Holloway, J. Leith, Jr., "Numerical Integration of a Nine-Level Global Primitive Equations Model Formulated by the Box Method," *Monthly Weather Review*, Vol. 95, No. 8, Aug. 1967, pp. 509–530.

Masuda, Y., "A Finite Difference Scheme by Making Use of Hexagonal Mesh-Points," *Proceedings of the WMO/IUGG Symposium on Numerical Weather Prediction, Tokyo, November 26–December 4, 1968*, Meteorological Society of Japan, Tokyo, Mar. **1969**, pp. 35–45.

Mintz, Yale, "Very Long-Term Global Integration of the Primitive Equations of Atmospheric Motion," *Proceedings of the WMO/IUGG Symposium on Research and Development Aspects of Long-Range Forecasting Boulder, Colo., 29 June–4 July 1964*, Secretariat of the World Meteorological Organization, Geneva, **1965**, pp. 141–167.

Neamtan, S. M., "The Motion of Harmonic Waves in the Atmosphere," *Journal of Meteorology*, Vol. 3, No. 2, June **1946**, pp. 53–56.

Okamura, Yashushi, "A Finite-Difference Scheme for the Primitive Equation Model With Special Emphasis on the Suppress of the Two-Grid Interval Noise," *Proceedings of the WMO/IUGG Symposium on Numerical Weather Prediction, Tokyo, November 26–December 4, 1968*, Meteorological Society of Japan, Tokyo, Mar. **1969**, pp. 1–11.

Phillips, Norman A., "Numerical Integration of the Primitive Equations on the Hemisphere," *Monthly Weather Review*, Vol. 87, No. 9., Sept. **1959**, pp. 333–345.

Rao, M. Sankar, and Umscheid, Ludwig, Jr., "Test of the Effect of Grid Resolution in a Global Prediction Model," *Monthly Weather Review*, Vol. 97, No. 9, Sept. **1969**, pp. 659–664.

Sadourny, Robert, Arakawa, Akio, and Mintz, Yale, "Integration of the Nondivergent Barotropic Vorticity Equation With an Icosahedral-Hexagonal Grid for the Sphere," *Monthly Weather Review*, Vol. 96, No. 6, June **1968**, pp. 351–356.

Vestine, E. H., Sibley, W. L., Kern, J. W., and Carlstedt, J. L., "Integral and Spherical-Harmonic Analysis of the Geomagnetic Field for 1955.0, Part 2," *Journal of Geomagnetism and Geoelectricity*, Vol. 15, No. 2, Aug. **1963**, pp. 73–89.

Washington, Warren M., and Kasahara, Akira, National Center for Atmospheric Research, Boulder, Colo., **1969** (private communication).

Washington, Warren M., and Kasahara, Akira, "A January Simulation Experiment With the Two-Layer Version of the NCAR Global Circulation Model," *Monthly Weather Review*, Vol. 98, No. 8, Aug. **1970**, pp. 559–581.

Williamson, David, "Integration of the Barotropic Vorticity Equation on a Spherical Geodesic Grid," *Tellus*, Vol. 20, No. 4, Nov. **1968**, pp. 642–653.

Williamson, David, "Numerical Integration of Fluid Flow Over Triangular Grids," *Monthly Weather Review*, Vol. 97, No. 12, Dec. **1969**, pp. 885–895.

CORRECTION NOTICE

Vol. 98, No. 4, Apr. 1970: p. 271, last par., 3d line, -1 should be read as the superscript instead of 1; p. 274, 1st line below equations (15), $((r-1)/\Delta t)$ should be read instead of $(r-1/\Delta t)$; p. 278, section 9, 22d line, baroclinic should be read instead of barotropic.